Understanding Knight shift in 2D Hubbard Model using Algorithmic Matsubara Integration(AMI)

by

© **Deep Gajera**

A thesis submitted to the School of Undergraduate Studies in partial fulfillment of the requirements for the degree of Bachelor of Science (Honours).

Department of Physics and Physical Oceanography

Memorial University

December 2023

St. John's, Newfoundland and Labrador, Canada

Abstract

The Knight shift is a critical probe in the study of high-temperature superconductivity. It provides insights into the interplay between electronic states and magnetic nuclei interactions. This research focuses on the Knight shift in the context of a 2D Hubbard model, exploring the interacting quantum systems and electronic correlations using a new computational tool called AMI (Algorithmic Matsubara integration). The Hubbard model provides a foundational framework for understanding electron-electron correlations, and the Knight shift emerges as a key observatory for characterizing these interactions due to its effects on the resonance frequency in the NMR experiments.

Specifically, we examine the suppression of the Knight shift, which signifies the formation of a partial gap in the density of electronic states. To comprehensively understand the behavior of electrons in the Knight shift conditions, we employ perturbation theory within the 2D Hubbard model framework. This approach establishes a clear relationship between susceptibility and temperature across various doping levels, chemical potential, and density of states.

Our research addresses the significance of half-filling in the 2D Hubbard model, examining the connections between the density of states and chemical potential for different doping levels. We also explored the relationship between the Hubbard interaction constant (U), magnetic susceptibility (χ_{sp}), temperature, and doping.

Acknowledgements

I would like to express my deepest gratitude and appreciation to my supervisor, Dr. James LeBlanc, for their invaluable guidance, unwavering support, and exceptional mentorship throughout the entire process of completing this thesis.

I would also present my gratitude to Dr. Mykhaylo Evstigneev and Dr. Qiying Chen for being my PHYS 490 A and B supervisors. They helped me in organizing my research thesis, maintaining the timelines for the thesis, preparing me for my research presentation, and guiding me throughout the process of writing my research thesis.

I deeply appreciate Michael Burke, Brad McNiven, and other members of Dr. LeBlanc's research group for discussing ideas, brainstorming, and providing valuable insights that enriched my research. Your diverse perspectives and thoughtful feedback helped me refine my arguments and expand my understanding of the subject matter.

I would also like to thank my parents for supporting me throughout my journey, they provided me with a great education and helped me in coming to Canada.

Table of contents

List of tables

List of figures

Chapter 1

Introduction

Tight-binding model provides a framework for understanding the behavior of electrons in a crystal lattice by considering the wave functions of individual atoms and their interactions with neighboring atoms [6]. However, the tight binding model only considers electron hopping from one site to another but doesn't account for electron-electron interactions. The 2D Hubbard model is a simplified theoretical model that accounts for the interplay between electron hopping and electron-electron interactions [5]. It is widely used to study the behavior of strongly correlated materials, such as high-temperature superconductors [2]. The Hubbard model is a perturbation of the tight-binding model where the coulomb potential can be treated as a perturbation to the Hamiltonian of the tight-binding model [12].

The Knight shift measures the change in the NMR frequency or resonance peak position when a material is subjected to an external magnetic field [1]. It directly reflects the local magnetic susceptibility of the atomic nuclei within the sample. The knight shift represents the additional shift in the resonance frequency of nuclear spins due to their interaction with the conduction electrons [1]. In superconductors, the

Knight shift can provide information about the formation of Cooper pairs and the onset of superconductivity. Changes in the Knight shift can help identify the critical temperature (Tc) at which a material becomes superconducting [8]. Understanding the suppression of the Knight shift and its relationship with the pseudo gap is critical for gaining insights into the mechanisms behind high-temperature superconductivity [1].

To understand the knight shift we need the magnetic susceptibility of the model which is induced due to the interaction of conduction electrons in the 2-D Hubbard model. A Many-body system is a system of a large number of particles (electrons) interacting due to coulomb force between them [11]. These complicated interactions between many electrons are also referred to as many-body problems which can be solved using the Feynman diagrams and Dyson's equation [10]. A Feynman diagram is a symbolic representation of the mathematical expressions describing the behavior and interaction of subatomic particles [11]. Hence, each of these interactions can be represented as an individual diagram. These diagrams are mathematically expressed using a mathematical tool called greens functions. Green's function provides a way to solve differential equations and describe the behavior of linear operators. In the context of many-body theory, Green's function is used to describe the behavior of particles within a many-particle system [10]. Moreover, Dyson's equation is an excellent way of converting these complicated interactions as a sum of irreducible simpler interactions. The Dyson equation captures the link between the self-energy and the Green's function. Where the self-energy represents the effects of interactions between particles on the properties of a single particle within the many-body system [11]. It accounts for the corrections to the bare properties of the particle due to its interactions with other particles. Now the next step is to solve these irreducible interactions.

In general, any interaction in a n-dimensional lattice can be expressed as a function of the position and time of the particle. However, when we are making these calculations in an infinite periodic lattice certain variable transformations can make our calculation exponentially simpler. In models like Hubbard and tight-binding, the interaction and its properties are usually expressed as a function of momentum vectors and frequencies which can be obtained by taking Fourier transfer of position and time. Since the Feynman diagrams are also mathematically expressed as a function of momentum vectors and frequencies it makes sense to keep everything in the same basis.

To include all the degrees of freedom and time we need to take an integral over position and time which is converted to again integrals over momentum vectors and frequencies. Algorithmic Matsubara Integration (AMI) is a tool for evaluating the frequency integrals that arise in the evaluation of Feynman diagrams [20]. Monte Carlo integration is used to evaluate the momentum-space integrals [15]. Using these tools we can compute spin susceptibility and try to understand the relationship between the spin susceptibility and temperature for different levels of doping for Knight shift.

Using a many-body system and perturbation tools in the Hubbard model, we tried to calculate the magnetic susceptibility for different sets of parameters. These kinds of studies have been previously performed using different computational tools where they have investigated the Hubbard model with different momentum vectors and frequencies. However, an investigation of the Knight shift using the Algorithmic Matsubara integration is performed for the first time since the AMI is a recently developed technique. This thesis consists of the method to use numerical integration tools (AMI and Monte Carlo Integration) to solve many-body problems in the 2-D Hubbard Model and evaluate knight shift as a function of temperature and the validity

of these results.

The motivation for the project was to understand the accuracy of AMI and which range of parameters are optimal for the practical application of the model. Throughout the project, we have used the Hubbard interaction constant U = 2. This particular parameter can be used for someone simulating a superconductor material with a low value of coulomb interaction or Hubbard constant such as Sr_2RuO_4 [16]. The next step of the process is to improve the model by adding the temperature dependence to the chemical potential and making the density of the state a fixed number. This will take us one step closer to the practical application of the model for different superconductors.

Chapter 2

Theory

2.1 Many-body physics

First, let's start with understanding the physics of many-body systems. Many-body physics is the physics of a microscopic system of particles interacting with each other based on laws of physics. The physical properties of microscopic systems of interacting particles are very difficult to calculate due incredibly intricate motions of microscopic particles [11]. The main problem in determining these properties is that they are continuously changing depending upon the changes in the surrounding particles and as the system has numerous particles. To simplify this problem, we can use the perturbation theory where we start with a simple system and add a small perturbation [14]. We can introduce quasi-particles to the system and try to convert the system into a non-interacting system of quasi-particles. Quasi particles are non-interacting and turn the system into a non-interacting system by shielding the real particles such as electrons. This prevents the coulomb interactions and excludes the interaction between the electrons [11]. Thus, the continuous changes of physical properties in the

interacting system turn into a non-interacting one as shown in Fig. 2.2.

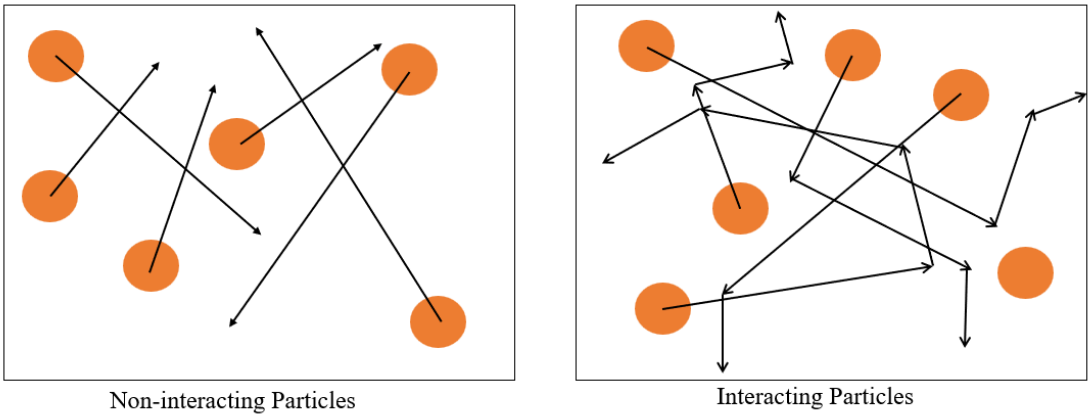

Figure 2.1: Two different types of systems of particles in many body systems: Non-interacting particles and Interacting system.

2.2 Self Energy

Self-energy is a concept that arises in the field of many-body theory, particularly in the context of quantum field theory and condensed matter physics. The self-energy represents the effects of interactions between particles on the properties of a single particle within a many-body system [11]. In quantum field theory, the self-energy is a correction to the bare mass or energy of a particle and it arises due to the particle's interactions with other particles. Due to this correction, the energy law for the quasi-particle changes as the mass changes [11]. So, let's denote the new mass as m^* and thus new energy is given by

$$\epsilon^*_{quasiparticle} = \frac{p^2}{2m^*} \quad \text{rather than being } \epsilon_{bareparticle} = \frac{p^2}{2m} \tag{2.1}$$

And by this definition and for the purpose of understanding self-energy is given by

$$\epsilon_{quasiparticle} - \epsilon_{bareparticle} = \epsilon_{self} \tag{2.2}$$

The self-energy plays a crucial role in many-body calculations, as it allows for the inclusion of interactions and their impact on the properties of single particles within a system. By accounting for the self-energy, one can obtain more accurate predictions for various physical quantities and phenomena in quantum field theory and condensed matter physics. However, calculating it is very tricky because the self-energy of a particle has to include all the possible interactions of elementary particles. Feynman Diagrams is one of the best representation that helps us understand all the possible interactions of elementary particles. Generally, self-energy is introduced through the concept of Green's functions which are the mathematical representation of Green's functions and Dyson's equation [11].

2.3 Non-interacting Green's Function

Although the system non-interacting system lacks interactions between the particles there are still other phenomena occurring in the lattice. The Green's function for the non-interacting part of the Hubbard model also known as zero temperature green's function is denoted as G_0 is a fundamental concept in many-body physics and condensed matter theory. The non-interacting Green's function encapsulates information about the single-particle properties of the system. The spectral function, which is related to G_0, gives insights into the allowed energy levels and their occupation [10].

The density of states is a crucial quantity in condensed matter physics, describing

the distribution of energy levels available to particles in a material [7]. The non-interacting Green's function is directly related to the density of states, and the DOS is often calculated from G_0 to understand the electronic structure of materials. The most basic and known Green function is the function for the non-interacting particle [11] and is given by

$$G_0^+(k, t_2 - t_1) = \theta_{t_2-t_1} e^{-i\epsilon_k(t_2-t_1)} \tag{2.3}$$

But we usually use the momentum space convention because it makes our calculations easy and in momentum space, Green's function is given by

$$G_0(k, \omega) = \frac{1}{\omega - \epsilon_k + i\Gamma} \tag{2.4}$$

where k is the momentum vector, ω is the frequency and ϵ_k is the energy [11] [10].

Since in theory, we start with a non-interacting model, the non-interacting Green's function is a good starting point for developing an interacting many-body system.

2.4 Tight Binding Model

This model is made up of electrons placed in a lattice and is allowed to move from one lattice site to another nearest neighboring site with an exchange in energy. This is a non-interacting model where the arrangement allows the electrons to interact with lattice sites but not other electrons [17]. The Hamiltonian in the tight-binding model is given by

$$T = \sum_{i,j,\sigma} t_{i,j} c_{i,\sigma}^\dagger c_{j,\sigma} \tag{2.5}$$

where $t_{i,j}$ is a hopping amplitude, $c_{i,\sigma}^\dagger c_{i,\sigma}$ are the creation and annihilation operators at site i. The zero temperature green's functions are derived from the Hamiltonian

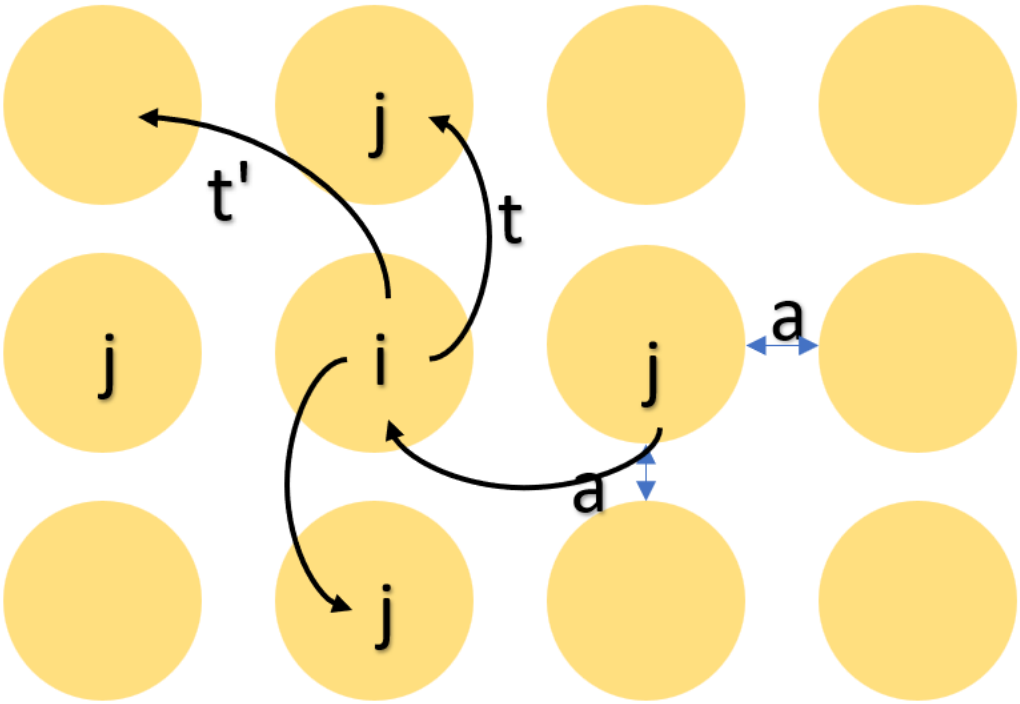

Figure 2.2: lattice site of a 2D Tight Binding Model

of the tight-binding model. Now let's see how we can use the non-interacting green functions to derive other physical properties of the tight-binding model [7].

2.4.1 Density of states in Tight Binding Model

It is a standard problem to derive the tight binding dispersion for a 2D square lattice including only nearest-neighbor hopping, using the results of this standard problem we know that energy in the tight binding 2D square lattice is given by

$$\epsilon_k = -2t[cos(k_x) + cos(k_y)] - \mu \tag{2.6}$$

where k_x, k_y are the momentum space coordinates and μ is the chemical potential [7]. and from equation 2.4

$$G_0 = \frac{1}{\omega_n - \epsilon_k + i\Gamma} \tag{2.7}$$

And the imaginary part of non-interacting Green's function can be obtained by the conjugate square method and is given by

$$ImG_0 = \frac{1}{\pi} \frac{\Gamma}{(\omega - \epsilon_k)^2 + \Gamma^2} \tag{2.8}$$

Where $\Gamma^2 \to 0^+$. The normalized imaginary part of the non-integrating green's function is also known as the spectral function and is defined by

$$A(k, \omega) = \frac{-1}{\pi} ImG \tag{2.9}$$

The spectral function can be used to understand the relationship between the density of states and Matsubara frequency by integrating the spectral function with respect to respective momentum axes k_x, k_y (here k_x, k_y are in units of the lattice constant). The normalized density of the state is given by

$$N(\omega) = \frac{1}{4\pi^2} \int_0^{2\pi} \int_0^{2\pi} A(k_x, k_y, \omega) dk_x dk_y \tag{2.10}$$

Using equation 2.6 for 2D lattice and substituting it in equation 2.8 and 2.9 and integrating the final equation 2.10 gives us Fig. 2.3.

Using the result of integration we can calculate the occupation number of the 2D square lattice using equation 2.11 and Figure 2.4 is the relationship between Occupation number and μ [7].

$$n = \int N(\omega) f(\omega) d\omega \tag{2.11}$$

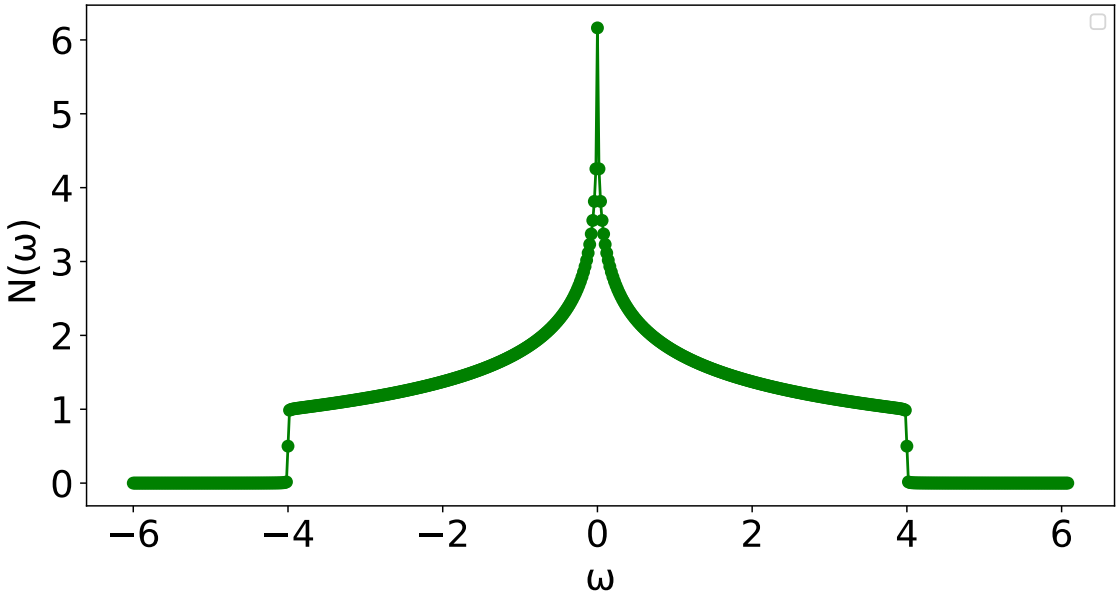

Figure 2.3: This figure shows the relationship between density of states and ω and the peak at $\omega = 0$ shows the Van Hove singularity.

where $f(\omega)$ is the ground state Fermi function and n is the Occupation number.

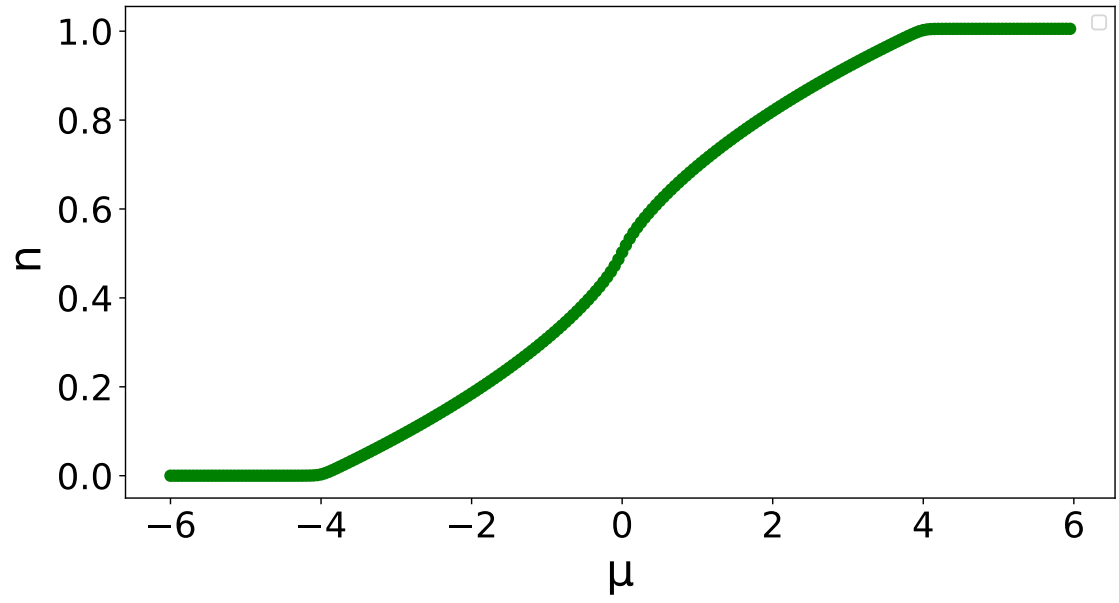

Figure 2.4: This figure shows the relationship between Occupation number (n) and μ and half filling is found at $\mu = 0$

2.5 Feynman Diagrams

By definition, the Feynman diagram is a picture or symbol representation of mathematics that is used to describe the behavior and interaction of subatomic particles. It was developed by American physicist Richard Feynman in 1948. Let's understand Feynman diagrams with some examples shown in Fig. 2.5 [11].

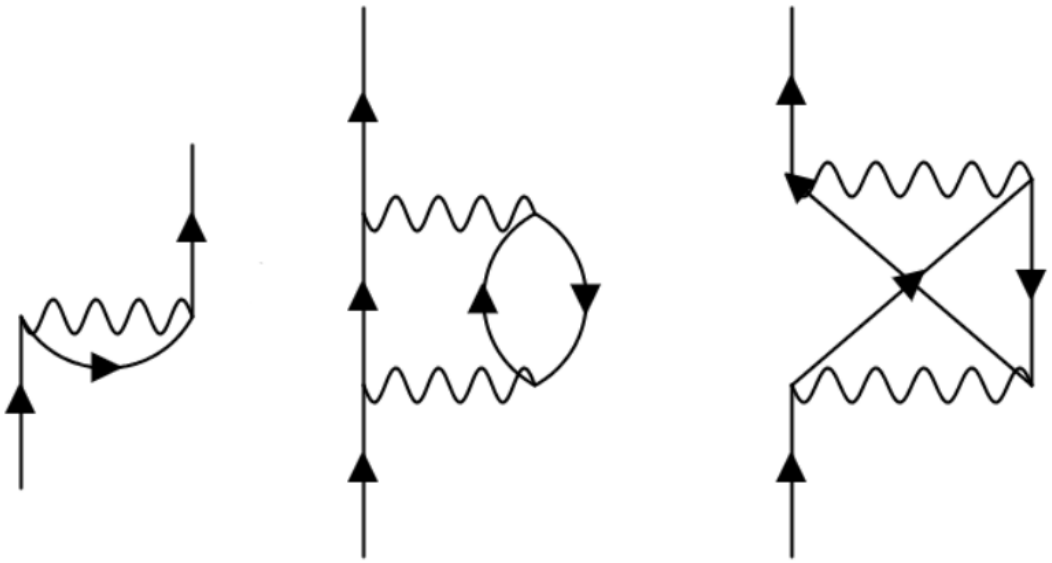

Figure 2.5: Few examples of the Feynman diagrams

The squiggly line represents the phonon and the straight line is the fermions. The Feynman diagram is based on the conservation laws and thus the main solids straight line after each interaction will have the same momentum vector and frequency [11]. The mathematical factor of the diagram elements is

$$\omega_n = \frac{(2n+1)\pi}{\beta} \tag{2.12}$$

These pictorial representations provide a physical interpretation of each term as a

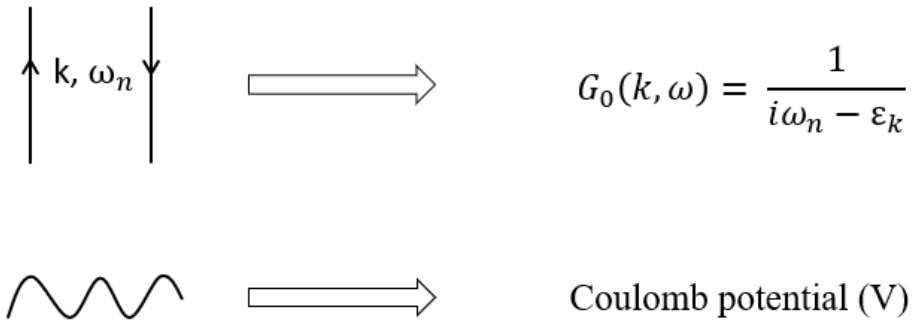

Figure 2.6: Feynman diagrams to their mathematical form

particular interaction of the particles and also help us in simplifying mathematics.

2.6 Matsubara Formalism

The Matsubara formulation is a mathematical framework used in quantum field theory and statistical mechanics, particularly in the context of finite-temperature calculations [19]. In this formulation, physical observable are often expressed as sums over discrete frequencies called Matsubara frequencies. These frequencies are typically associated with imaginary time, and the idea is to perform calculations in the Euclidean time domain rather than in real time. This allows for easier handling of temperature effects in quantum systems.

In the Matsubara formulation, time is treated as an imaginary quantity (it takes values along the imaginary axis of the complex plane). This is done to simplify calculations involving thermal effects. The Matsubara frequencies are a set of discrete

values of imaginary time [19]. The Matsubara frequencies for fermions are given by

$$\omega_n = \frac{(2n+1)\pi}{\beta} \tag{2.13}$$

where β is the inverse temperature (1/kT) and n is an integer. These frequencies correspond to the allowed energy levels at finite temperatures.

Many physical observable can be expressed as sums over Matsubara frequencies, which makes it easier to calculate thermodynamic properties and correlation functions at finite temperatures. After calculations are done in the Matsubara formalism, one often needs to perform an analytical continuation to obtain real-time results, which are the physically observable quantities.

The main reason to use this particular formulation is that it simplifies calculations by discretizing the energy spectrum, incorporating temperature effects, and providing a framework for systematic calculations of thermal observables [11]. While it may introduce complexities related to working with imaginary time, these are often more manageable than the challenges associated with real-time finite-temperature calculations in quantum field theory.

Matsubara frequencies come into play when expressing the self-energy and Green's functions in terms of these frequencies [19]. The self-energy, $\Sigma(k, \omega_n)$, is determined using the interaction processes by summing over all the irreducible self-energy of relevant Feynman diagrams or employing perturbation theory techniques. The full Green's function, G(k, iω_n), and the self-energy, $\Sigma(k, \omega_n)$, are typically functions of both momenta (k) and Matsubara frequencies (ω_n).

2.7 Green's Function at finite temperatures

It provides information about the propagation of particles, their interactions, and their response to external fields. In the context of quantum field theory, Green's function is typically defined as the expectation value of a time-ordered product of field operators [10]. Now if we conduct an experiment where we leave a particle at position x1 in an interacting system at time t1 in its ground state then at some time t2 we will find the particle at position x2 [11]. The probability amplitude of this experiment is given by $iG(x_2, x_1, t_2 - t_1)$. Similarly, the probability amplitude in the momentum-frequency space is given by the green function

$$G(k, \omega) = \frac{1}{\omega - \epsilon_k - \sum(k, \omega) + i\delta_k} \tag{2.14}$$

where $\sum(k, \omega)$ is the sum of all proper self-energy or irreducible self-energy [10] [11]. Moreover, for the case of a non-interacting system the $\sum(k, \omega) = 0$ which takes us back to $G_0(k, \omega)$(non-interacting Green's function).

2.8 Dyson's equation

Dyson's equation is a key tool for studying interacting quantum systems because it connects Green's function, self-energy, and Feynman Diagrams, and it plays a central role in understanding various phenomena, including electronic structure, many-body effects, and collective excitation in condensed matter physics and quantum field theory [11]. Dyson's equation allows us to go from a system of quasi-particle or non-interacting systems to a system of interacting particles by providing a mathematical framework. This mathematical framework of the behaviour of particles in quantum

mechanics is encoded in Dyson's equation which is derived from the framework of Green's functions.

Dyson's equation plays a key role in Perturbation Theory as it starts with a bare electron or the known non-interacting system ($G_0(k,\omega)$) and systematically computes higher-order corrections and obtains an expanded description of the system's behavior in terms of interaction strengths [10].

Dyson's equation introduces the concept of self-energy in terms of Green's functions. The self-energy, in many-body physics, explains the collective properties of the system, quasi-particle formation, and other emergent phenomena. A system of electrons can be in different quantum interactions described by Feynman Diagrams and each of these interactions will change the self-energy of the system. Hence, the self-energy of a system is the collection of all proper self-energy parts or irreducible self-energy of all the possible interactions [11]. Derivation of the self-energy of the system by adding all the irreducible self-energy gives Dyson's equation 2.20. Let's start with a simple non-interacting case which is $G_0(k,\omega)$ and is represented by $\uparrow$ and add an irreducible interaction to it

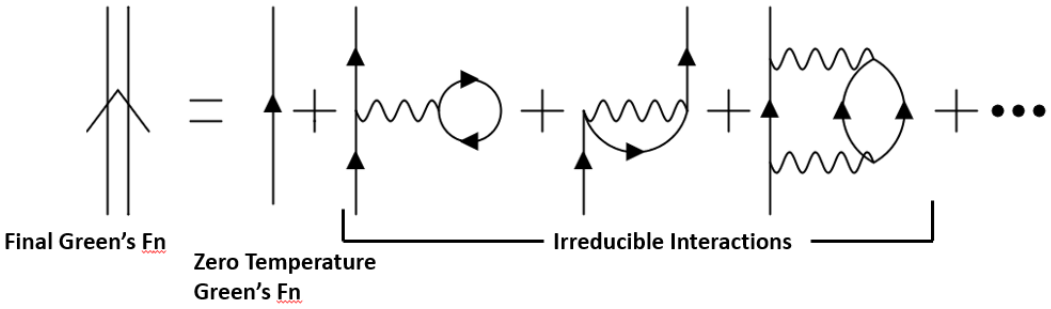

Figure 2.7: we are summing over all repetition of irreducible parts,

Now let's solve this mathematically using the Green function and self-energy of a

single irreducible interaction.

$$G = G_0(k,\omega) + G_0(k,\omega)\Sigma(k,\omega)G_0(k,\omega) + G_0(k,\omega)\Sigma(k,\omega) \\ G_0(k,\omega)\Sigma(k,\omega)G_0(k,\omega) + ... \tag{2.15}$$

here $G(k,\omega)$ is the Green's function of the dressed electron and the $G_0(k,\omega)$ is the function of non-interacting or bare electron and $\Sigma(k,\omega)$ is the self-energy of the system. This is a sum of all the possible interactions which are the sum over all the repetition of all irreducible self-energy parts [11]. We can rewrite this equation as

$$G = G_0(k,\omega) + G_0(k,\omega)\Sigma(k,\omega)[G_0(k,\omega) + G_0(k,\omega)\Sigma(k,\omega)G_0(k,\omega) + ...)] \tag{2.16}$$

Or

$$G = G_0(k,\omega) + G_0(k,\omega)\Sigma(k,\omega)G(k,\omega) \tag{2.17}$$

Or

$$G(k,\omega)[1 - \Sigma(k,\omega)G_0(k,\omega)] = G_0(k,\omega) \tag{2.18}$$

Hence,

$$G(k,\omega) = \frac{G_0(k,\omega)}{1 - \Sigma(k,\omega)G_0(k,\omega)} \tag{2.19}$$

Or

$$G(k,\omega) = \frac{1}{\frac{1}{G_0(k,\omega)} - \Sigma(k,\omega)} \tag{2.20}$$

This is the final form of the Green's function at a finite temperature which we previously saw in eq. 2.14 [11]. Now we can use this equation to solve for physical observables like the magnetic susceptibility of the model.

2.9 2-D Hubbard model

The Hubbard model is an approximation model for describing the interaction of electrons placed at specific lattice sites. The electrons in the Hubbard model are governed by the Hubbard Hamiltonian [12].

$$H = \sum_{i,j,\sigma} t_{i,j} c^{\dagger}_{i,\sigma} c_{j,\sigma} + U \sum_{i} n_{i,\uparrow} n_{i,\downarrow} \tag{2.21}$$

where $t_{i,j}$ is a hopping amplitude, $c^{\dagger}_{i,\sigma} c_{j,\sigma}$ are the creation and annihilation operators at site i and U is the Hubbard interaction constant. When studying the Hubbard model, we aim to understand the complex interplay between electron-electron interactions and hopping kinetics. The hopping term (-t) allows electrons to move between neighboring lattice sites, promoting the de-localization of charge carriers. It describes the kinetic energy associated with the motion of electrons in the lattice. The on-site Coulomb interaction term (U) accounts for the repulsion between electrons occupying the same lattice site [10]. It represents the potential energy cost for two electrons with opposite spins to occupy the same orbital, reflecting the principle of electron-electron repulsion. The chemical potential (μ) term controls the electron density in the system. By adjusting μ, one can control the number of electrons in the lattice and study phenomena such as doping or electron addition/removal.

The Hubbard model is built upon the tight-binding model where the second term ($U \sum_i n_{i,\uparrow} n_{i,\downarrow}$) is a small perturbation added to the tight-binding model [14]. This term involves the effects due to electron-electron interaction on the site. We can adjust the parameter U to better understand the relationship between the strength of Coulomb potential and its effects on the system.

2.10 Magnetic susceptibility

Calculating the magnetic susceptibility in a 2D Hubbard model involves considering how the system responds to an external magnetic field. The Hubbard model describes interacting electrons on a lattice, and its magnetic susceptibility is a measure of the system's susceptibility to being magnetized. There are many different ways of finding the magnetic susceptibility of the 2D Hubbard model however we are going to use linear response theory which relates the response of a system to external fields to its equilibrium correlation functions [3]. The spin magnetic susceptibility (or spin correlation function)χ_{sp} is given by

$$\chi_{sp}(q, i\Omega_n) = \int_0^\beta dt \sum_r e^{-iqr} \langle S_z(r,t) S_z(0,0) \rangle \tag{2.22}$$

where

$$S_z(r,t) = n_\uparrow(r,t) - n_\downarrow(r,t) \tag{2.23}$$

and $\beta = 1/T$ and the $S_z(0,0)$ is the initial spin at the time (t=0) and position (r=0). The system is left to interact and after the time t the particle is at the position and its spin is $S_z(r,t)$ [18]. Now, it is very difficult mathematically to solve with position and time as our variables and we perform the Fourier transform on position space to convert it to momenta space and similarly convert the time to frequency variable.

2.11 Knight Shift

In the 2D Hubbard model, the knight shift refers to a phenomenon in condensed matter physics related to the behavior of localized electron spins (magnetic moments) in a lattice [13]. In conductors and semiconductors, localized electrons can interact with

other electrons within the lattice site causing shifts in the nuclear magnetic resonance (NMR) frequency, which is a technique used to study the magnetic properties of a material [13]. When these localized electrons are mobile, such as in a metallic state, they can move through the lattice, and their motion is influenced by the interactions with other electrons and lattice vibrations (phonon).

Understanding the suppression of the Knight shift and its relationship with the pseudo gap is critical for gaining insights into the mechanisms behind high-temperature superconductivity and indicates fewer available electronic states for interaction with magnetic nuclei [1]. Moreover, changes in the Knight shift can help identify the critical temperature (T_c) at which a material becomes superconducting. This phenomenon may provide clues about the nature of Cooper pairs and the role of strong electronic correlations in the superconducting state.

However, in the case of the 2D Hubbard model, we see Knight shift by setting up certain parameters. One of these parameters is half half-filling of the lattice sites also known as a half-filled system. Half-filling in the 2D Hubbard model is related to the momentum vector q through the behavior of the electronic states at the Fermi level. At half-filling, there is one electron per lattice site on average, which means that the Fermi level lies exactly in the middle of the non-interacting band structure [12]. This specific electron-filling condition has important consequences for the momentum dependence of the electronic states and the behavior of the system. However, we can also use other occupation numbers to understand the behavior of the knight shift for different values of chemical potentials.

2.11.1 How to compute K_s for 2D Hubbard model.

We have already been through how to apply perturbation theory to the tight-binding model to include the $e^- - e^-$ interactions. We can physically observe the Knight shift in the 2D Hubbard model by observing the magnetic susceptibility of the model. However, in order to observe the shift we need to compute the susceptibility at the momenta vector and frequency to zero [1]. Hence we can say that

$$K_s \propto \chi_{sp}(q = (0, 0), \Omega = 0) \tag{2.24}$$

Our 2D Hubbard model is an infinite space model and thus it's not ideal to calculate the Knight shift of each lattice site. Similarly, we need to provide enough time for the model to interact and provide accurate results. Hence we take the spatial average and temporal average to compute the random phase approximation of the magnetic susceptibility. We can use eq 2.25 and 2.26 to compute these averages.

$$\chi_{sp}(Q = 0, \Omega) \rightarrow \int e^{-i(Q=0).r} \chi(r, \Omega) dr \tag{2.25}$$

$$\chi_{sp}(Q, \Omega = 0) \rightarrow \int e^{-i(\Omega=0)\tau} \chi(r, \tau) d\tau \tag{2.26}$$

There are many numerical integration tools that can be used to compute these integrals like DiaMC (Diagrammatic Monte Carlo) but we are specifically focused on using Algorithmic Masturbate integration (AMI) to compute these integrals over the frequency of eq. 2.26 [20]. Now let's see what numerical tools we used for this project and how they compute these integrals.

Chapter 3

Methods and Numerical integration tools

3.1 AMI

3.1.1 Theory

Arithmetic Matsubara integration is a numerical technique used to approximate integrals over the Matsubara frequencies in the context of finite-temperature calculations. It allows for the evaluation of thermal properties without explicitly summing over an infinite number of frequencies. Let's understand it with an example of the pair-bubble at finite temperature [11].

Polarization bubble at finite temperature

We will solve for pair bubble for a non-zero temperature using the residue theorem. we can see that a photon with momentum q and frequency Ω interacts and splits

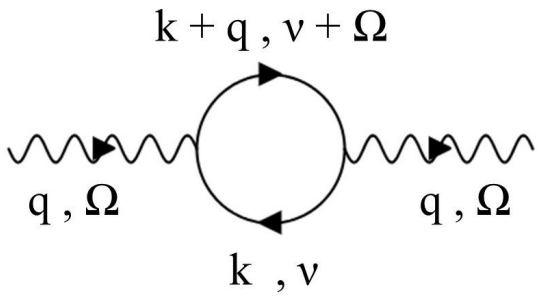

Figure 3.1: Polarization bubble also commonly known as pair-bubble

into an electron and positron pair where the electron has k + q momentum and ν + Ω frequency and the positron has k, ν. Moving forward the pair reunites and the interaction results in a photon with momentum q and frequency Ω and this process is called a polarization bubble or pair bubble.

Formation of mathematical equation

Firstly lets start with writing this pair bubble in mathematical form and defining variables. Using the Diagram dictionary from table 14.1 from [11] for Fig. 3.1 we can express the fermion interaction on terms of Green's function. Mainly we will use the equation for $\circlearrowright$ (k,Ω_n) which is

$$fermion\ loop - - > -1 \tag{3.1}$$

$$Internal\ (k, \nu_m) - - > \sum_k or \int \frac{d^3k}{(2\pi)^3}, \frac{1}{\beta} \sum_{m=-\infty}^{+\infty} \tag{3.2}$$

$$\circlearrowright - - > \frac{1}{\beta} \sum_{m=-\infty}^{+\infty} G_0(k, \nu_m) e^{i\nu_m 0^+} \tag{3.3}$$

$$\curvearrowleft - - > \frac{1}{\beta} \sum_{m=-\infty}^{+\infty} G_0(k+q, \nu_m + \Omega_n) e^{i(\nu_m + \Omega_n)0^+} \tag{3.4}$$

Mathematically pair-bubble is denoted by Π_0(q,Ω) and is given by

$$\Pi_0(q, \Omega_n) = (-1) \times 2 \times \frac{d^3k}{(2\pi)^3} \times \frac{1}{\beta} \sum_m G(k, i\nu_m) G(k+q, i\nu_m + i\Omega_n) \tag{3.5}$$

Here q is the momentum transfer, iΩ_n is the imaginary frequency, k is the momentum of the particles in the system, G(k,iν_m) is the single-particle Green's function, which describes the behavior of a single particle (here it's the positron with momentum k and frequency ν) in the system [11].

$$\Pi_0(q, \Omega_n) = -2 \int \frac{d^3k}{(2\pi)^3} \frac{1}{\beta} \sum_{m=-\infty}^{(+\infty)} \frac{1}{i\nu_m - (\epsilon_k - \mu)} . \frac{1}{i\nu_m + i\Omega_n - (\epsilon_{k+q} - \mu)} \tag{3.6}$$

Solving equations using residues theorem

Let's start with defining a function $A(x)$ by

$$A(x) = \frac{1}{x - (\epsilon_k - \mu)} . \frac{1}{x + i\Omega_n - (\epsilon_{k+q} - \mu)} \tag{3.7}$$

we can see that A(iν_n) is the partial frequency part of the 3.6 and now keeping k constant let's solve for frequencies. Let's first understand some maths involved in the derivation using the function A(x) and Fermi function and try to evaluate integration of A(x) and Fermi function from $-\infty$ to ∞.

$$\int_{\infty}^{-\infty} A(x) f(x) dx \tag{3.8}$$

As we know for a function of a complex variable with integration limits as[$-\infty$, ∞] can be transformed into a contour and we can use the residue theorem to evaluate the integration over the contour.

Using properties of residue theorem we can write our 3.8 as

$$\oint_{C'} A(x)f(x)dx = 2\pi i(\sum_{ResF(x)} A(x)f(x) + \sum_{Resf(x)} A(x)f(x)) \tag{3.9}$$

We can use some unique properties of the Fermi function here to simplify this equation further. Here,

$$f(x) = \frac{1}{e^{\beta x}+1} \tag{3.10}$$

This function will help us with Matsubara Formalism as $f(x) = \infty$ when $x = \frac{i\pi}{\beta}(2n+1)$, where n = 0, $\pm$ 1, ... and these values of n will give a set of poles that we can use as we know how to apply the residue theorem to the Fermi function.

Now coming back to eq. 3.8 using the notations from fig 3.2 we can write the second term of the summation as

$$\oint_{C} A(x)f(x)dx = 2\pi i \sum_{Resf(x)} A(x)f(x)) \tag{3.11}$$

From the properties of the residue theorem, we know that the integral around C' goes to zero and C' approaches ∞. Now our eq. 3.8 will look like

$$\oint_{C'} = \oint_{C} A(x)f(x)dx + 2i\pi \sum_{ResF(x)(poles)} A(x)f(x)) = 0 \tag{3.12}$$

Which can also be expressed as

$$\oint_{C} A(x)f(x)dx = -2\pi i \sum_{ResF(x)(poles)} A(x)f(x)) \tag{3.13}$$

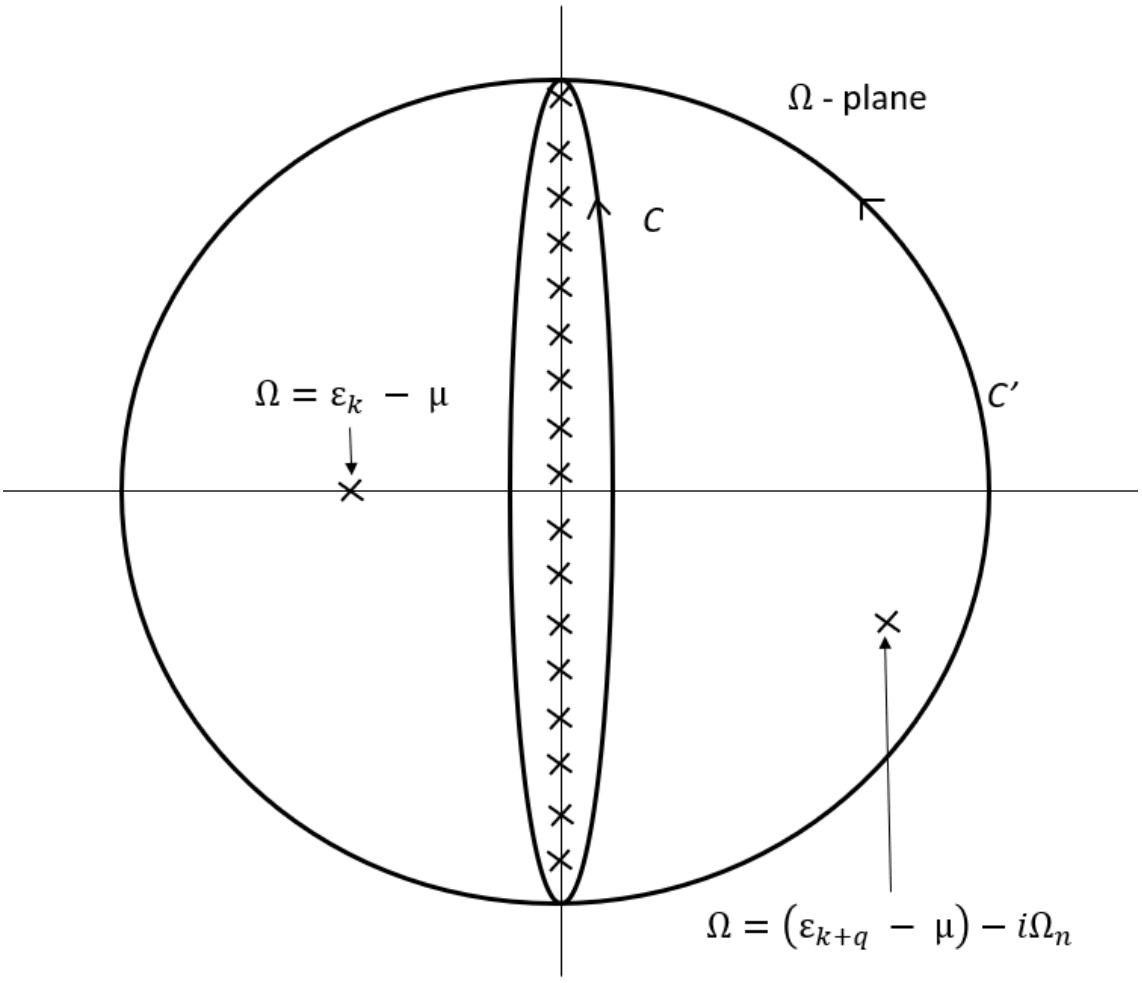

Figure 3.2: This is the contour used for the residue theorem in the case of the finite temperature calculation.

Using eq. 3.8 equation we can write $A(i\nu_m)$ as

$$\frac{1}{\beta}\sum_{m=-\infty}^{m=+\infty} A(i\nu_m)) = \sum_{ResF(x)(poles)} A(x)f(x)) \tag{3.14}$$

Now using all these equations we can write this final relation which we can use to solve eq. 3.6,

$$\sum_{m=-\infty}^{m=+\infty} A(i\nu_m)) = \frac{-\beta}{2\pi i}\oint_C A(x)f(x)dx \tag{3.15}$$

Now using eq. 3.15 in 3.6 we get

$$ResA(x)f(x) = \begin{cases} \frac{f(\epsilon_k-\mu)}{\epsilon_k-\mu+i\Omega_n-(\epsilon_{k+q}-\mu)} & x = \epsilon_k - \mu \\ \frac{f(\epsilon_{k+q}-\mu-i\Omega_n)}{\epsilon_{k+q}-\mu-i\Omega_n-(\epsilon_k-\mu)} & x = \epsilon_{k+q} - \mu - i\Omega_n \end{cases} \tag{3.16}$$

Using all the above equations we can rewrite our main equation 3.6

$$\Pi_0(q,\Omega_n) = -2\int \frac{d^3k}{(2\pi)^3}(ResA(x)f(x)_{x=\epsilon_k-\mu} + ResA(x)f(x)_{x=\epsilon_{k+q}-\mu-i\Omega_n}) \tag{3.17}$$

$$\Pi_0(q,\Omega_n) = -2\int \frac{d^3k}{(2\pi)^3}(\frac{f(\epsilon_k-\mu)}{\epsilon_k+i\Omega_n-\epsilon_{k+q}} + \frac{f(\epsilon_{k+q}-\mu-i\Omega_n)}{\epsilon_{k+q}-i\Omega_n-\epsilon_k}) \tag{3.18}$$

$$\Pi_0(q,\Omega_n) = -2\int \frac{d^3k}{(2\pi)^3}(\frac{f(\epsilon_k-\mu)-f(\epsilon_{k+q}-\mu-i\Omega_n)}{\epsilon_k+i\Omega_n-\epsilon_{k+q}}) \tag{3.19}$$

Now let's simplify this equation by adding and subtracting '$f(\epsilon_k-\mu)f(\epsilon_{k+q}-\mu-i\Omega_n)$' to the numerator,

$$\Pi_0(q,\Omega_n) = 2\int \frac{d^3k}{(2\pi)^3}\frac{(f(\epsilon_{k+q}-\mu-i\Omega_n)(1-f(\epsilon_k-\mu))-f(\epsilon_k-\mu)(1-f(\epsilon_{k+q}-\mu-i\Omega_n)}{(\epsilon_k+i\Omega_n-\epsilon_{k+q})} \tag{3.20}$$

Now let's make a final substitution by taking k+q = -k which will make $f(\epsilon_{k+q}-\mu-i\Omega_n = f(\epsilon_{-k}-\mu-i\Omega_n) = f(\epsilon_k-\mu-i\Omega_n)$ and $\epsilon_{-k} = \epsilon_k$ which finally gives us

$$\Pi_0(q,\Omega_n) = 2\int \frac{d^3k}{(2\pi)^3}f(\epsilon_k-\mu)(1-f(\epsilon_{k+q}-\mu-i\Omega_n)[\frac{1}{i\Omega_n-\epsilon_k+\epsilon_{k+q}}-\frac{1}{i\Omega_n+\epsilon_k-\epsilon_{k+q}}] \tag{3.21}$$

This final form of the derivation is in Matsubara frequency space which is imaginary frequencies. Now we need to convert it to a real frequency version. After the final

conversion, we will get [11]

$$\pi_0^T(q,\Omega) = f^+(\Omega)\Pi_0(q,\Omega+i\delta) + f^-\Pi_0(q,\Omega-i\delta) \tag{3.22}$$

which is a very similar form as eq.2.22 Now finally we can write that the Knight shift and spin susceptibility is given by

$$K_s \propto \chi_{sp}(q,\Omega) = \pi_0^T(q,\Omega) \tag{3.23}$$

This process can be repeated for all the different Feynman diagrams which are made up of irreducible interactions and can be solved using Dyson's equation and final form of the spin susceptibility eq. (3.23).

3.1.2 How the AMI code works

We just saw the mathematics involved in the evaluation of the frequency integral of Green's functions for the Feynman diagrams. Now let's understand how the code works. This section is heavily based on the "Algorithmic Matsubara integration for Hubbard-like models" [20] as we are using the computation method (AMI) of this paper for our project. We start with the general starting point where we have to evaluate an integral over k_n and ν_n for any given Green's functions of the Feynman diagram. Currently, our sample is in two spaces, momentum space, and frequency space and we will use the AMI to convert it to only momentum space. For the conversion of the space we need to evaluate the integral over the set of frequencies ($\nu_n = \nu_1, \nu_2, ...$), and what remains is the sample with integration variable (k_n). The

most general form of the Feynman diagram is

$$\Pi = \frac{U^{n_\nu}}{\beta^n} \sum_{k_n} \sum_{\nu_n} \prod_{i=1}^{N} G^i(\epsilon^i, \Omega^i) = U^{n_\nu} \sum_{k_n} I^n \tag{3.24}$$

here Π is just a dummy variable representing the final result of the computation of a given diagram, n_ν is the order of the diagram which refers to the number of vertices and n refers to the number of summation over the frequencies ν_n and internal momenta k_n and N is the number of the internal lines of the Feynman diagram which again can be represented as a Green's functions [20]. we can rewrite this equation as two separate summations where the integration over the frequency term is

$$I^n = \frac{1}{\beta^n} \sum_{\nu_n} \prod_{i=1}^{N} G^i(\epsilon^i, \Omega^i), \tag{3.25}$$

here we the Green's function of the ith line is represented as

$$G^i(\epsilon^i, \Omega^i) = \frac{1}{\Omega^i - \epsilon^i} \tag{3.26}$$

here Ω is the frequency and the ϵ is the free particle dispersion. where ϵ^i is a function of k_i and the now using the conservation of momentum and energy we can express the momentum and frequencies as a linear combination of internal and external components of the frequencies and momentum.

$$k_i = \sum_{a=1}^{b} \alpha_a^i k_a \tag{3.27}$$

and

$$\Omega^i = \sum_{a=1}^{b} i\alpha_a^i \nu_a \tag{3.28}$$

The coefficients α_i^a is one of the three values [-1,0,1]. Using this form of equation we can write Green's function of ith line as an array of length b+1 of the form

$$G^i(\Omega^i) \rightarrow [\epsilon^i, \vec{\alpha}^i] \tag{3.29}$$

this will help us transform our main equation 3.25

$$\prod_{i=1}^{N} G^i(\epsilon^i, \Omega^i) \rightarrow [[\epsilon^1, \vec{\alpha}^1]; [\epsilon^2, \vec{\alpha}^2]; [\epsilon^3, \vec{\alpha}^3]; ...; [\epsilon^N, \vec{\alpha}^N]] \tag{3.30}$$

Since our array of the Green's function is of size (b+1) the size of this array is $N \times (b+1)$. Now we have our eq. 3.25 as a summation of products of Green's function of the ith line of the Feynman diagram. Now let's simplify this one to more time and calculate one frequency at a time. Hence, we begin our algorithm with this final subdivision of the equation 3.25 to a summation over a single frequency ν_y and the remaining frequencies $\nu_n \neq \nu_y$ Hence

$$I^n = \sum_{[\nu_n], \nu_n \neq \nu_y} I_y = \sum_{[\nu_n], \nu_n \neq \nu_y} \sum_{\nu_y} \prod_{i=1}^{N} G^i(\epsilon^i, \Omega_b^i) \tag{3.31}$$

Now, we can start the computation by first identifying the simple poles of Green's functions which is given by

$$z_y^i = -\alpha_y^i(-\epsilon^i + \sum_{a=1, a \neq y}^{b} i\alpha_a^i \nu_a) \tag{3.32}$$

This is a pole of the ith Green's function with respect to the frequency ν_y and it exists if its coefficient $\alpha_y^i \neq 0$. The total number of these poles are given by

$$P_y = \sum_{i=j}^{N} |\alpha_y^j| \tag{3.33}$$

Now we can represent Green's function with the total number of poles in them and the set of poles can be represented as $z_y^{j_a}$ where $a = [1, 2, .., P_y]$ and under the assumption that all the poles are simple the final residue of each of these poles is given by

$$\alpha_y^{j_a} \prod G^i(\alpha_y^i z_y^{j_a} + \sum_{a \neq y} i\alpha_a^i \nu_a) \tag{3.34}$$

Now we can use the residue theorem on the poles with the help of the Fermi function and the poles that we just defined.

$$\sum_{\nu_y} F(i\nu_y) = \beta \sum_{z_y} f(z_y) Res[F(z)]_{z_y} \tag{3.35}$$

where the Fermi function is used in the same symbolic representation is given by

$$f(z_y^{j_a}) = \frac{1}{\sigma e^{-\beta \alpha_y^{j_a} \epsilon^{j_a}} + 1} \tag{3.36}$$

where σ is just a sign function based on the number of fermionic frequencies such as if the number of these frequencies is odd then $\sigma = -1$ and for all the other cases its $\sigma = 1$. Now using the residue theorem in the final array form of the general equation

3.25 of the Feynman diagrams given by equation3.31, we get

$$I_y = \alpha_y^{j_1}\beta f(z_y^{j_1}) \prod_{i\neq j_1} G^i(\alpha_y^i z_y^{j_1} + \sum_{a\neq y} i\alpha_a^i \nu_a) + \alpha_y^{j_2}\beta f(z_y^{j_2}) \prod_{i\neq j_2} G^i(\alpha_y^i z_y^{j_2} + \sum_{a\neq y} i\alpha_a^i \nu_a) + ... + \alpha_y^{j_{P_y}}\beta f(z_y^{j_{P_y}}) \prod_{i\neq j_{P_y}} G^i(\alpha_y^i z_y^{j_{P_y}} + \sum_{a\neq y} i\alpha_a^i \nu_a) \tag{3.37}$$

This final equation will evaluate all the frequency integrals by applying the residue theorem for all the poles of Green's functions [20]. Hence, now we are only left with the integral over the momentum space which is represented by summation over the set of momentum k_n. Please refer to "Algorithmic Matsubara integration for Hubbard-like models" [20] for the details of the numerical method and the code itself can be found on the Github of Dr. James LeBlanc [9].

3.2 Monte Carlo Integration

Monte Carlo Integration is a numerical integration method that performs calculations with a random set of numbers. It is mainly used for definite integral and the random numbers are always numbers in the limits of the integration. Integration is performed at randomly chosen points and is averaged over the number of times the integration is performed. Monte Carlo integration is mostly used to evaluate high-order integrals [15]. We can use it to evaluate the integral over the momentum vectors k_n.

We chose Monte Carlo integration because it's one of the best methods to solve multidimensional integrals [4]. This is how a simple Monte Carlo integration works:

let's try integrating some function f(x) that we want to integrate from a to b.

$$F(x) = \int_a^b f(x)dx \tag{3.38}$$

Then we will use random points lying in range [a,b] to perform the interactions which

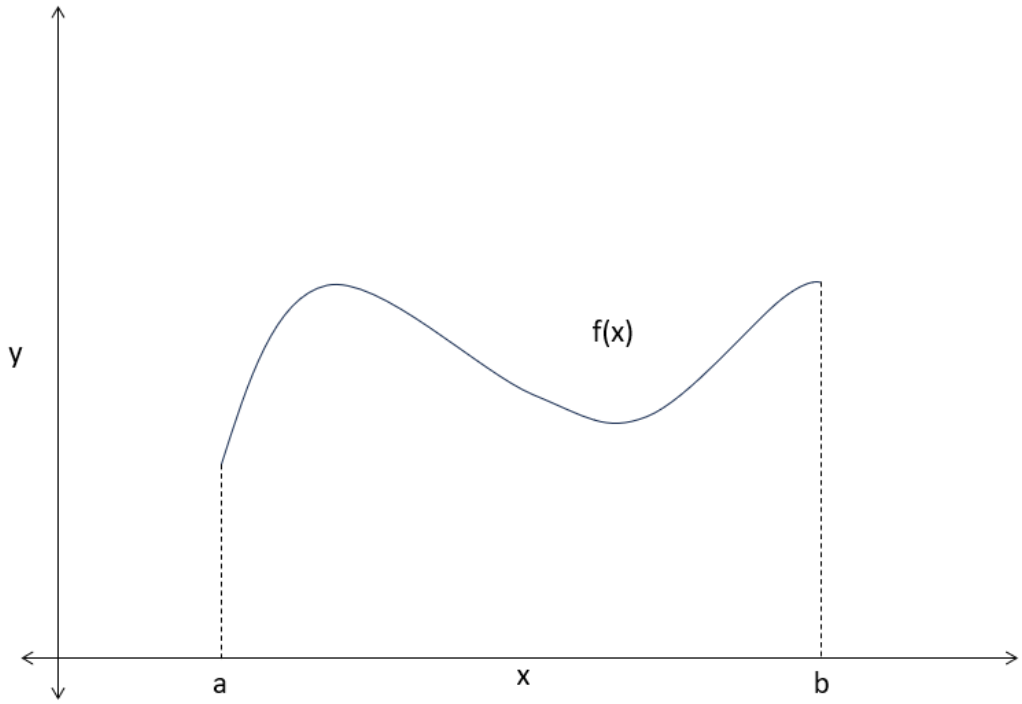

Figure 3.3: An example problem to demonstrate the Monte Carlo integration approach on a simple definite integral.

looks like

So using the Monte Carlo approach over the area A with N different point in area A chosen randomly gives us Fig. 3.4 and the average of all these individual integration gives a approximate value of F(x)

$$I = F(x) = \int_a^b f(x)dx = (b-a)\frac{1}{N}\sum_{i=1}^{N} f(x_i) \tag{3.39}$$

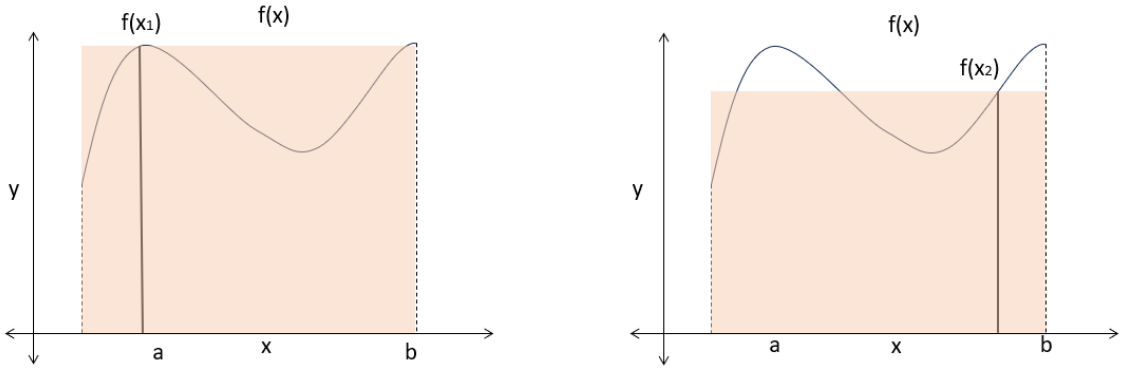

Figure 3.4: Here x_1 and x_2 are two randomly selected number between [a,b] and the shaded region represents the area under the curve which is the result of the integration.

Chapter 4

Results

4.1 Creating a known 2D Hubbard model using AMI

We started with understanding the interaction between electrons present in a two-dimensional lattice using the Hubbard model. As we know Feynman diagrams describe interactions between electrons and AMI uses the residue theorem to compute the internal Matsubara sums for different Feynman diagrams. I used the AMI code [9] provided by Dr. James Leblanc for different variables and ran the algorithm to find χ_{uu}, χ_{ud} cases, and total χ. We started with creating a 2D Hubbard model and performing calculations for the spin susceptibility with specific external variables as shown in table 4.1. Here β is the temperature, Reμ and Imμ is the real and imaginary part of chemical potential, kdim is the dimensionality of the lattice or model, kx, and ky are the momentum vectors components, and Reω and Imω are the real and imaginary parts of the Matsubara frequency.

β	Reμ	Imμ	H	kdim	kx	ky	Reω	Imω
5	0.01	0	0	2	3.141593	3.141593	0	-15.079645 to 15.079645

Table 4.1: Specific external variables used to get the susceptibility of the 2D Hubbard model

Using these parameters and running them for up-up and up-down cases we get results as spin susceptibility of the model for up-up and up-down cases [1]. The final susceptibility is given by

$$\chi_{spfinal} = \chi_{sp[uu]} - \chi_{sp[ud]} \tag{4.1}$$

Using equation 4.1 we can get the final susceptibility with respect to Matsubara frequency and the final result is shown in Fig.4.1.

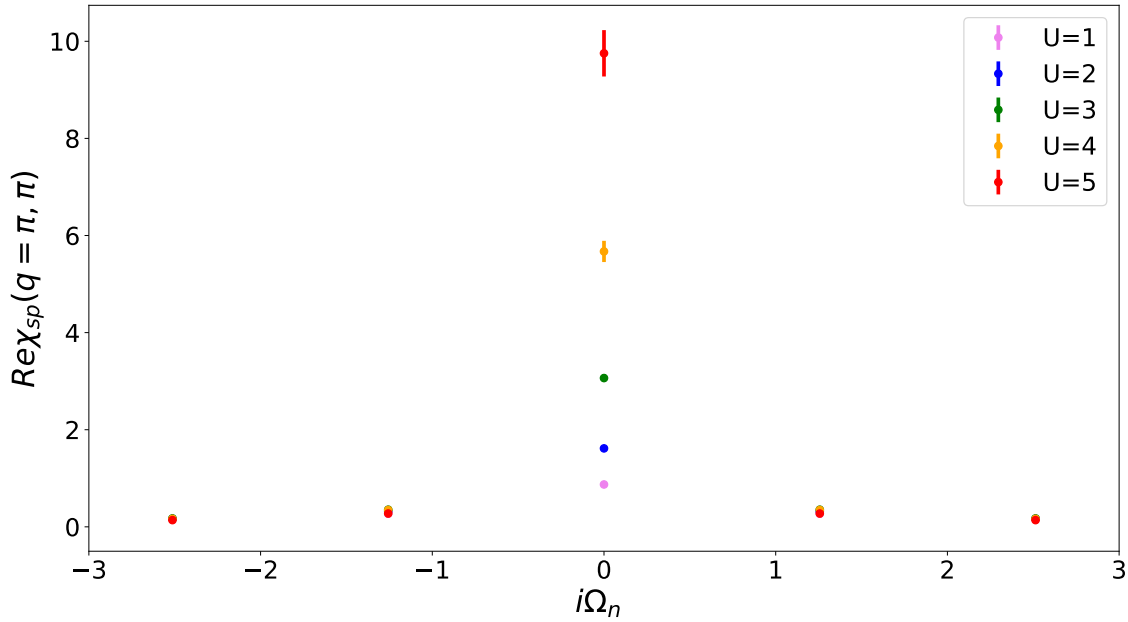

Figure 4.1: $Re\chi_{sp}(q = \pi, \pi)$ with respect to Matsubara frequency ($i\Omega_n$) for different values of the U. U here is the ratio of Hubbard interaction constant and hopping amplitude [U/t].

So, from these results, we can see that there is one single peak at $\omega = 0$ and that as the value of U increases the error in the susceptibility increases. This error can

be decreased by running the model for longer times but we are more focused on the practical use of the model to compute knight shift. So, using this observation we will focus on susceptibility at $\omega = 0$ and for U = 2.

4.2 Relationship between χ_{sp} and Temperature

In the next step, we tried to get the relationship between temperature and spin susceptibility for same the momentum vector q = (π, π) at $\omega = 0$ and for U =[1,5]. Hence our external variables will look like

β	Reμ	Imμ	H	kdim	kx	ky	Reω	Imω
0 to 20	0.01	0	0	2	3.141593	3.141593	0	0

Table 4.2: Specific external variables used to get the susceptibility of the 2D Hubbard model to get relationship between χ_{sp} vs β for ω=0.

The results that we get after using AMI on all the different Feynman diagrams using the external variables from Table 4.2 are shown in Figure 4.2.

All these results are previously calculated using different numerical integration methods and can be found in many different research papers as these results are building blocks or starting points for exploring 2D Hubbard model. Moreover, to see the accuracy of our calculation using AMI we compare our results with the results of "Tracking the Footprints of Spin Fluctuations: A MultiMethod, MultiMessenger Study of the Two-Dimensional Hubbard Model" paper's Fig. 14 which shows antiferromagnetic static susceptibility for the same external parameters as ours and the results are shown in Figure 4.3 [18].

From Fig. 4.3 we can see that the results obtained from AMI overlap with many previously used different methods of determining this particular relationship for U= 2.

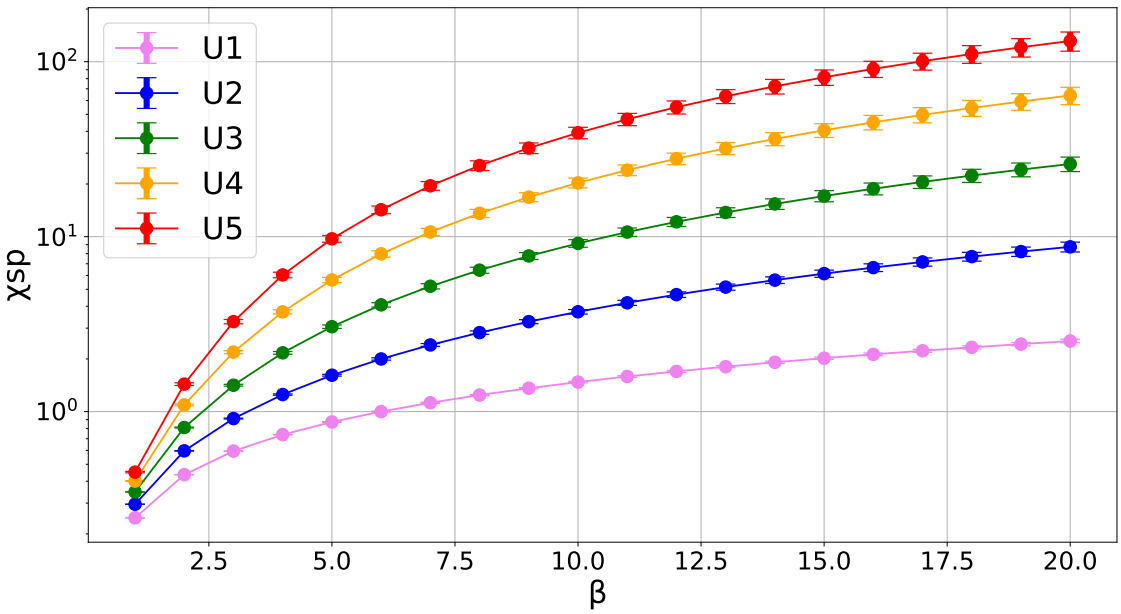

Figure 4.2: $Re\chi_{sp}(q = \pi, \pi), i\Omega_0$ with respect to β for different values of the U. U here is the ratio of Hubbard interaction constant and hopping amplitude [U/t].

Our data is particularly aligning with DQMC (Determinant Quantum Monte Carlo) and all the different methods start diverging after $\beta = 10$. After this particular point the data is not properly approximated and thus we have used this same range of β for all our calculations which matches with previously obtained data.

Hence, this comparison showed us that our results from AMI are reasonable and overlap with previously obtained results with different numerical analysis models. The main reason for this comparison is that AMI has not been previously used to compute the knigth shift or magnetic susceptibility so this helps us validate our results and were can make further adjustments to the parameters to compute Knight shift.

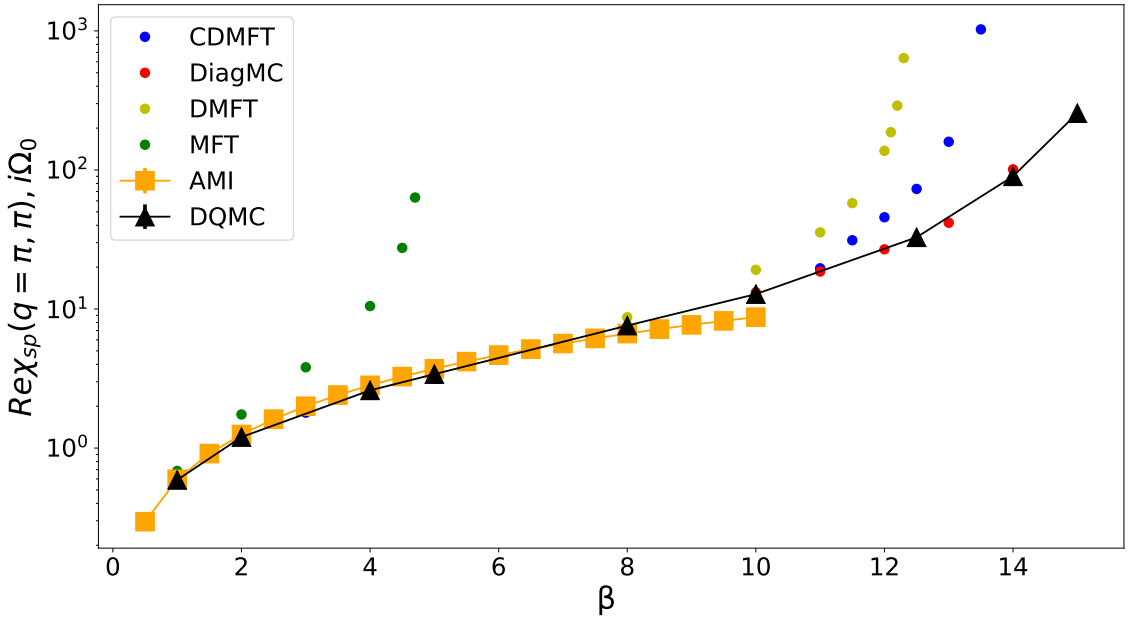

Figure 4.3: Comparing our results of change in $Re\chi_{sp}(q = \pi, \pi), i\Omega_0$ with respect to β for U = 2 with results of reference [18] (Fig.14) on a log scale. It's important to note that there was a missing factor of 2 in the reference paper's results and it's mentioned in the paper so we made the same adjustment in our results to match the domain of both the data.

4.3 Setting up parameters for Knights shift

Now the next step is to run the same model for external parameters of knights shift which happens at q = (0,0) [1]. So the external variables are set to the values shown in the table 4.3

β	Reμ	Imμ	H	kdim	kx	ky	Reω	Imω
0 to 20	0.01	0	0	2	0	0	0	0

Table 4.3: Specific external variables used to get the susceptibility of the 2D Hubbard model to get relationship between χ_{sp} vs β for knigths shift conditions.

The final result for the χ_{sp} is shown in Figure 4.4 where the pink triangles show the results obtained at q = (0,0) and the orange squares show the results obtained with q = (π, π). These results are for U = 2, $t' = 0$ and $\omega = 0$.

Since the trend of the χ_{sp} for two different momentum vectors are similar the local magnetic susceptibility for the conditions of knights shift is looking good. The conditions for observing the Knight shift in the 2D Hubbard model can depend on various factors, including temperature, electron-electron interactions, and carrier concentration (doping level). To reduce the complexity and reduce the computation time some of these parameters need to be fixed for our calculations.

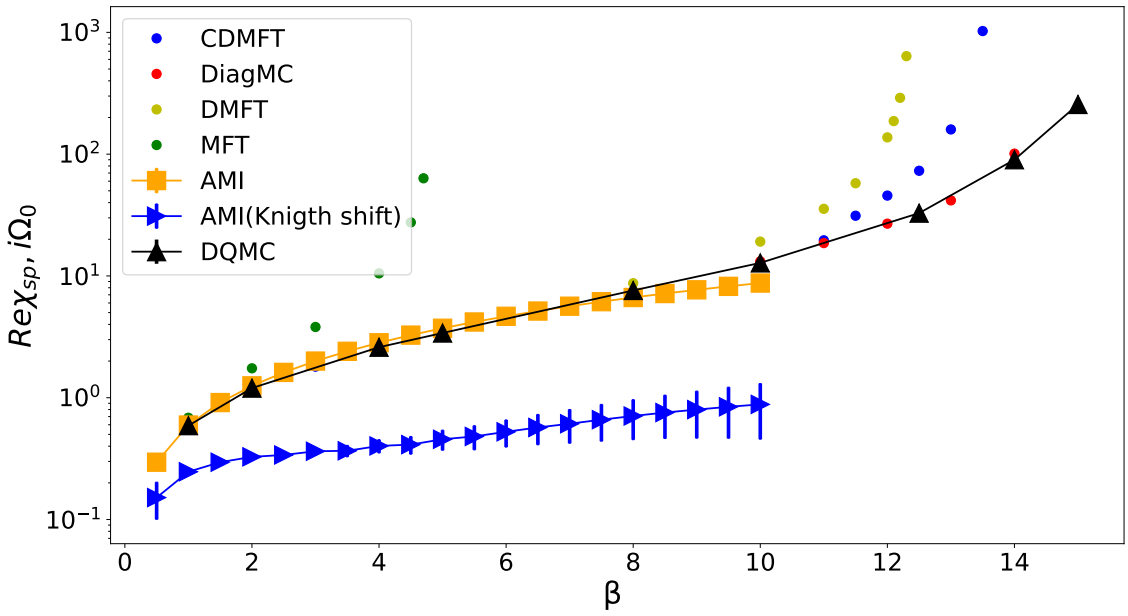

Figure 4.4: comparing magnetic susceptibility (χ_{sp}) for $[(q = \pi, \pi), i\Omega_0]$ and $[(q = 0, 0), i\Omega_0]$ to check the validity of our results for Knight shift and make sure that they are in the predicted range.

4.4 Introducing next nearest neighbour hopping (t' = -0.3)

We discussed in the Tight binding model that the energy is given by eq. 2.6 where t is the hopping parameter between nearest neighbors and $t' = 0$ for this equation.

However, in reality, there are hopping between the nearest atoms, the next nearest atom, and so on. Thus, the energy equation will change with the introduction of a new term that constitutes for next nearest interactions and will look like eq. 4.2

$$\epsilon_k = -2t[cos(k_x) + cos(k_y)] - 4t'[cos(k_x)cos(k_y)] - \mu \tag{4.2}$$

This also changes all the calculations of density of state and occupation number and

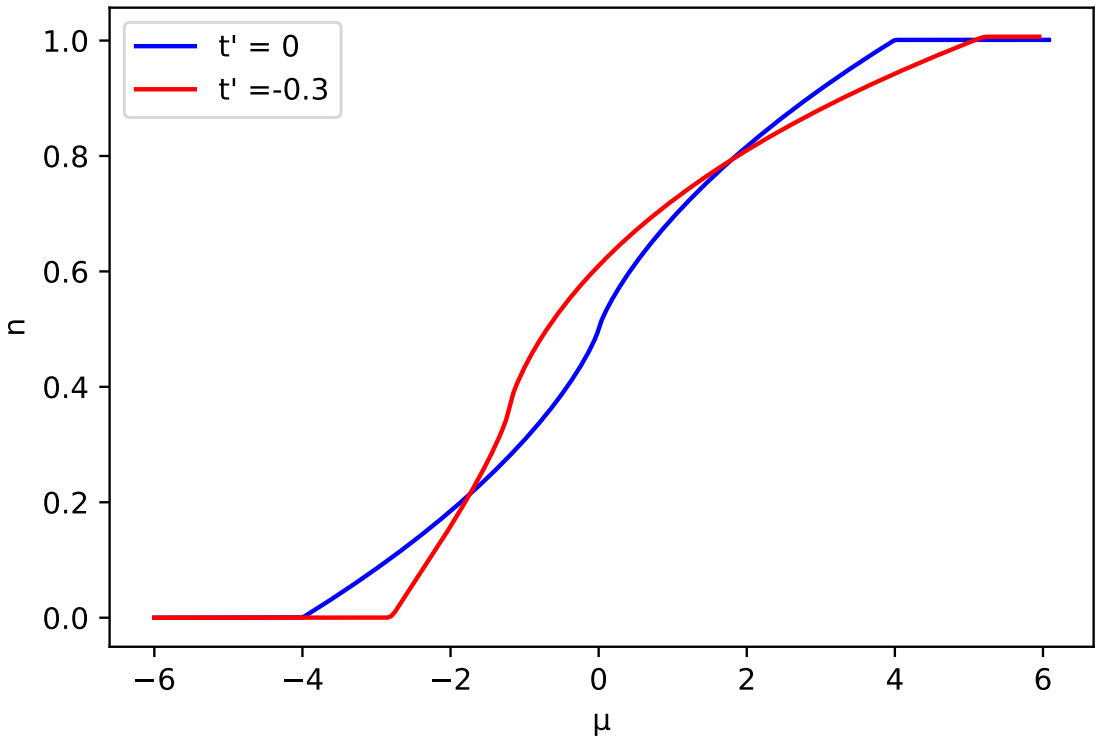

Figure 4.5: Relationship between n(occupation number) and μ for two different value of t'.

will provide a completely new relationship between n and μ. So when we repeat the numerical calculation of section 2.4.1 as there will be significant change in ϵ_k after introducing t' term to the original equation in 2.4.1. Figure 4.5 shows the comparison of occupation number n for two different values of t'. There are two ways of checking if the results are correct; first that the occupation number is continuously increasing

with μ and we also notice that the occupation number is 0.5 at $\mu = 0$ for $t' = 0$ or only first nearest neighbors interacting which is a known result.

After the introduction of second nearest neighbour the relationship occupation number and μ has changed and in order to compare the susceptibility in two cases one parameter (occupation number) is kept constant. Hence, for occupation number n = 0.2,0.3,0.4,0.5, and 0.6 we have two different set of values of μ for two cases.

Using the setup for Knights shift from section 4.3 and putting all these values of μ in the external variable table. The figure 4.4 is for t'= 0 and U =2 but this also means that it is for n = 0.5. Now we have a set of n for which we have two set μ respectively. Hence, we need to adjust the external variable individually for each value of n for both values of t.

μ(t=0)	n(t=0)	$\mu(t^{'} = -0.3)$	n($t^{'} = -0.3$)
-1.86	0.2	-1.8	0.2
-1.06	0.3	-1.4	0.3
-0.44	0.4	-1.1	0.4
0	0.5	-0.7	0.5
0.42	0.6	-0.05	0.6

Table 4.4: Specific external variables for μ for specific occupation number (n) from fig.4.5 for two different hopping constants used to get the susceptibility of the 2D Hubbard model to get the relationship between χ_{sp} vs β for Knight shift conditions.

Using the different values of the chemical potential (μ) as a function of the occupation number (n) for the external variables for AMI and computing the 2D Hubbard model for two hopping constants gives as Fig. 4.6 and Fig. 4.8. These graphs depict the relationship between $Re\chi_{sp}(q = 0, 0), i\Omega_0$ and β for two different hopping constants and occupation numbers. The Fig. 4.7 and Fig. 4.9 are showing the same results in $Re\chi_{sp}(q = 0, 0), i\Omega_0$ vs temperature(T) form which makes it easier to compare with previously obtained Knight shifts results from other computational methods and conditions. Now let's discuss our results.

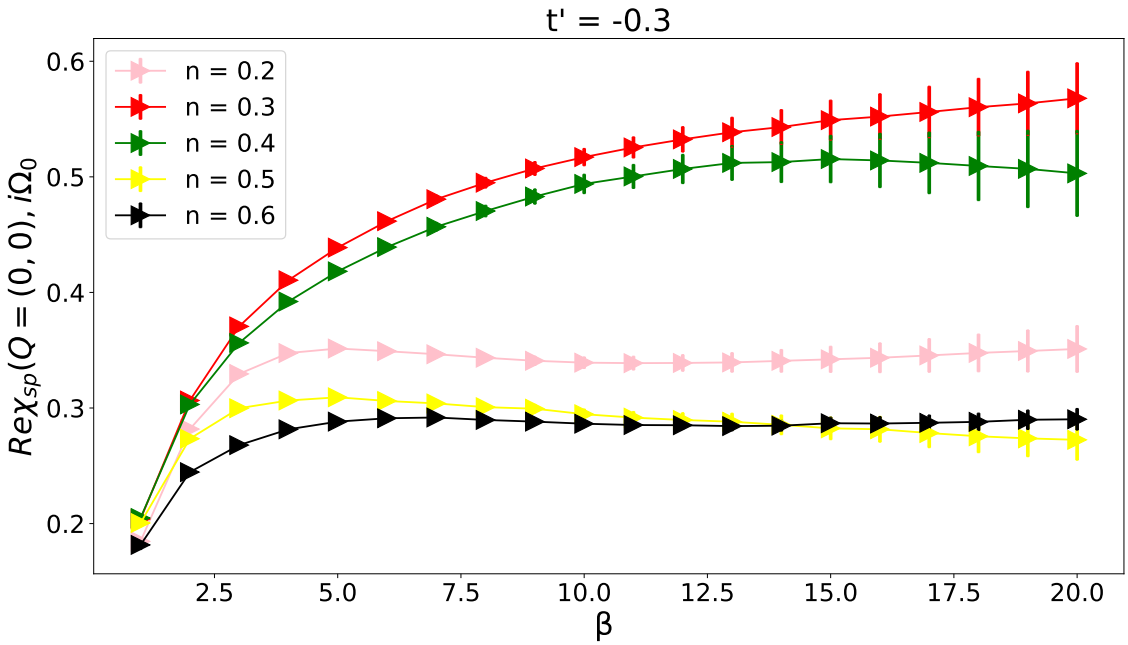

Figure 4.6: Relationship between Magnetic susceptibility $\chi_{sp}[(q = 0, 0), i\Omega_0]$ and β for different occupation number(n) when t' = -0.3

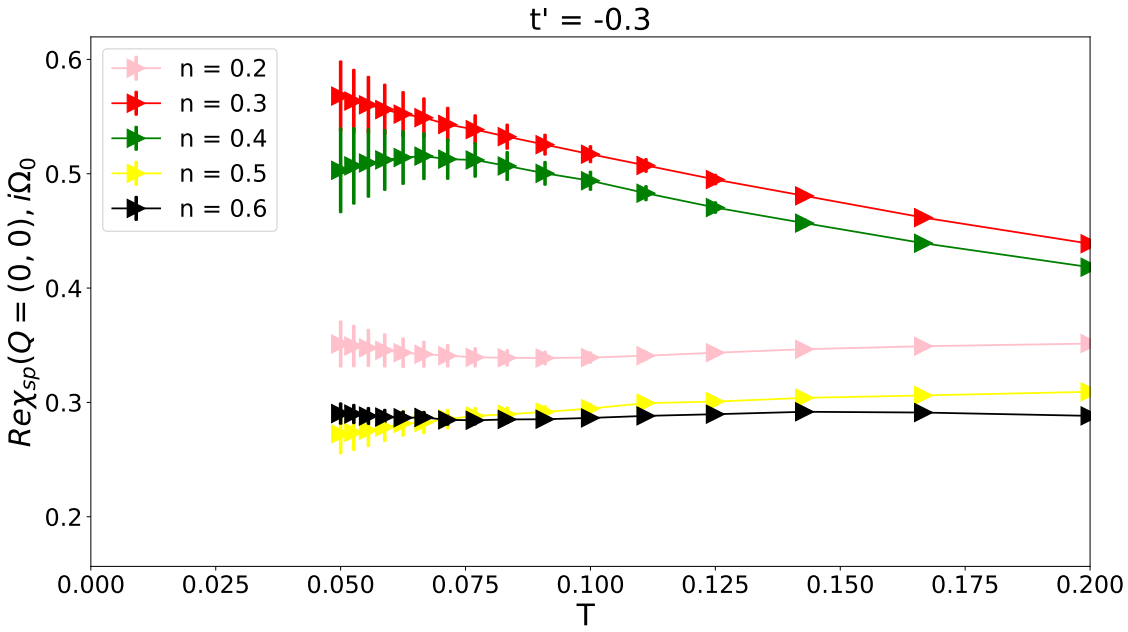

Figure 4.7: Relationship between Magnetic susceptibility $\chi_{sp}[(q = 0, 0), i\Omega_0]$ and temperature(T) for different occupation number(n) when t' = -0.3

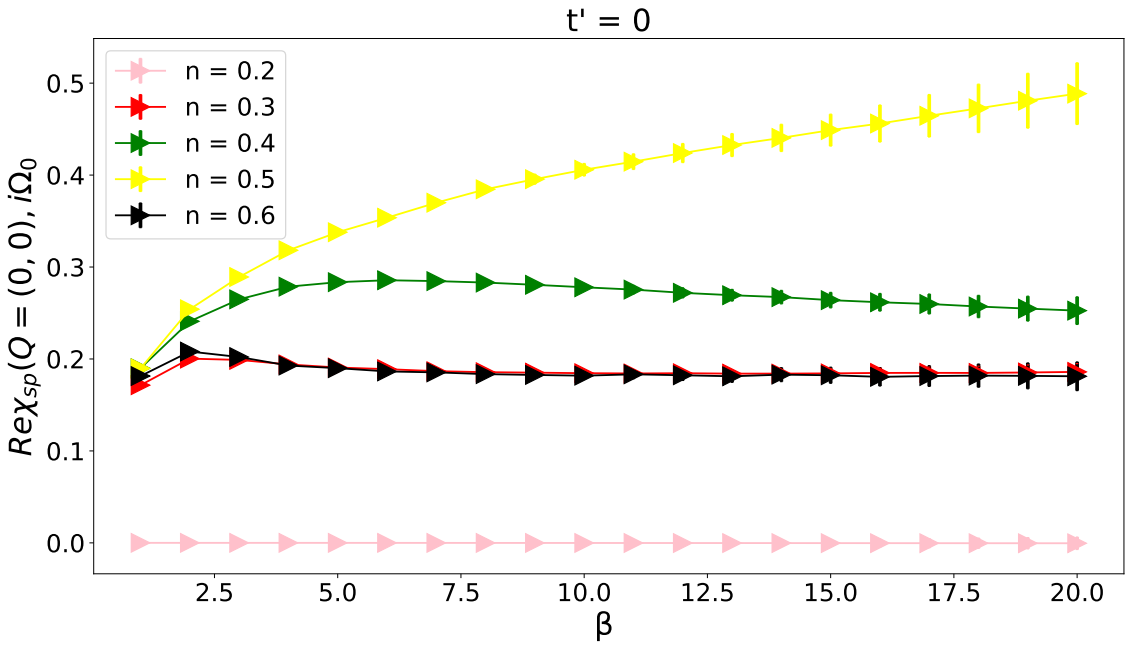

Figure 4.8: Relationship between Magnetic susceptibility $\chi_{sp}[(q=0,0),i\Omega_0]$ and β for different occupation number(n) when $t'=0$

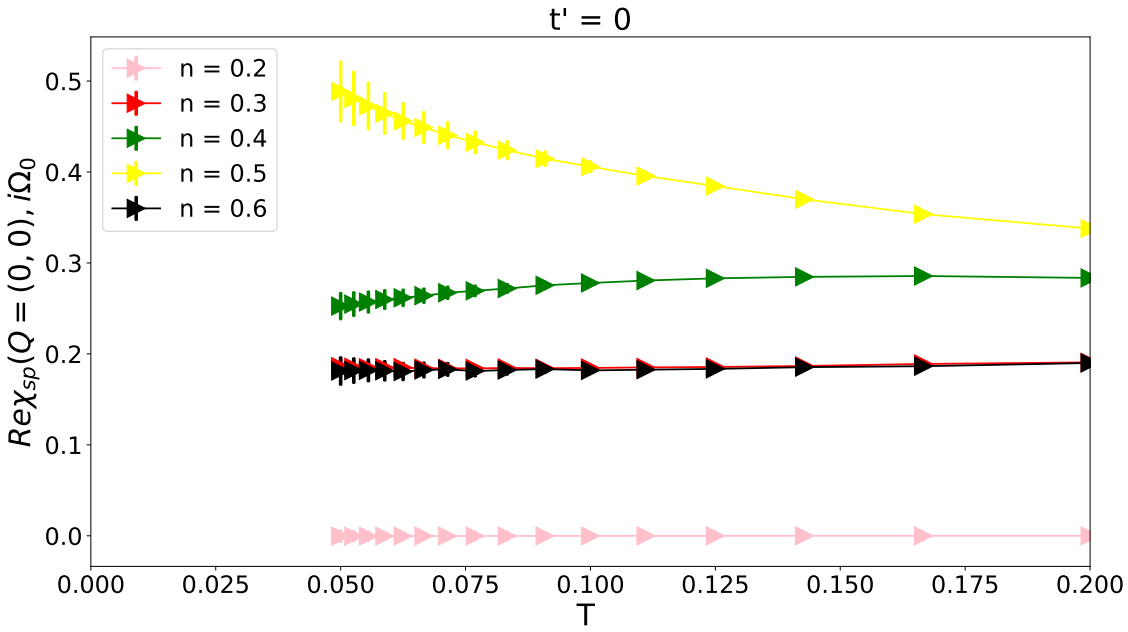

Figure 4.9: Relationship between Magnetic susceptibility $\chi_{sp}[(q=0,0),i\Omega_0]$ and temperature(T) for different occupation number(n) when $t'=0$

Chapter 5

Conclusion

5.1 Discussion

We have successfully computed the Knight shift in a 2D Hubbard model using the new numerical tool (AMI) and Monte Carlo Integration. We know this because the Knight shifts for $t' = 0$ and occupation number (n) = 0.5 half-filling conditions is a known result. At half-filling in the Hubbard model, the number of electrons is exactly equal to the number of lattice sites [12]. Each site is occupied by one electron on average. The strong on-site repulsion prevents two electrons from occupying the same site, as they would have to have opposite spins due to the Pauli exclusion principle. This means that at half-filling, the only way electrons can arrange themselves is to have one electron per site, each with an opposite spin to its neighbor. This arrangement leads to an antiferromagnetic ordering. The antiferromagnetic correlations are strong, leading to a higher magnetic susceptibility. For these reasons, we anticipate that the results we computed are a good approximation of the expectation values.

When we make all those adjustments and run the AMI code we are expected to

produce results like Fig. 5.1. Currently, although, some of the results show similar progressions, the particular dip in the K_s as the temperature decreases in missing, and this accuracy of K_s or χ_{sp} can only be achieved with proper adjustments of the parameters. In our current results, we can see a pseudo gap in Fig.4.7 for occupation number 0.4 and in Fig.4.9 for occupation number 0.5. We might also need to lower the temperature to see the pseudo gap more clearly in our future calculations.

5.2 Future Work

Although this project shows the working model of using AMI (Algorithmic Matsubara Integration) to compute frequency integrals of green's functions of Feynman diagrams it is still incomplete. Hubbard model is a rather complicated model due to a wide range of parameters to play with and as we were using fixed parameters for approximations of the results the accuracy of our model is not up to the mark yet.

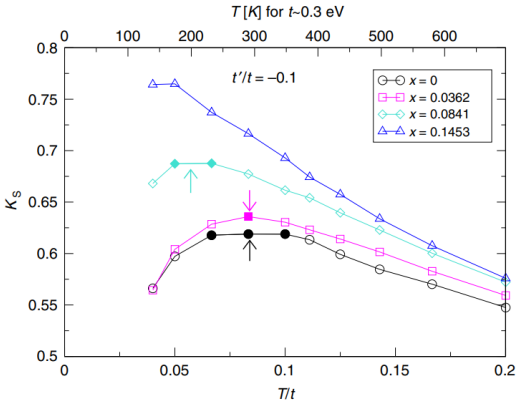

Figure 1 | Knight shift. Knight shift $K_S \propto \chi_m$ as a function of temperature T/t (lower x axis) for a series of doping levels computed at $U = 6t$, $t' = -0.1t$ obtained from 8-site DCA. Filled symbols: the peak positions of the Knight shift. Arrows: onset of normal state pseudogap obtained by analytical continuation of the single particle spectral function at $K = (0, \pi)$. Upper x axis: T/t in units of Kelvin assuming $t \sim 0.3$ eV.

Figure 5.1: Figure of Knight shift from [1] https://doi.org/10.1038/ncomms14986

Our results are based on many assumptions like our occupation numbers are changing with respect to chemical potential as seen in the table 4.4 for two hopping constants. We are interested in the behavior of the Knight shift with temperature to understand and more accurately ensure that the AMI is computing the equations

accurately. However, for practical applications, we need the occupation number related to the total number of electrons to be constant and the chemical potential is a function of temperature and for each value of temperature the values of chemical potential will change for two hopping constants. This will completely change the external variable table since the chemical potential will be determined by the Fermi-Dirac equation3.10. After making all these adjustments in the parameters, we are expected to get something similar to the previously obtained Knight shift results shown in Fig. 5.1 in [1].

Lay summary

The goal of this was to use the newly developed Algorithmic matsubara integration(AMI) tool to compute the Knight shift in the 2D Hubbard model. Imagine atoms as tiny magnets. When we apply a magnetic field to the material, the atoms respond by shifting their behavior slightly. The Knight shift is related to nuclear magnetic resonance (NMR), a technique used to understand the magnetic properties of a material. Here we are trying to create similar conditions as metals using the 2D Hubbard model.

In order to study the Knight shift we need to study the magnetic susceptibility of the material or (in our case) the model. To find the susceptibility we need to account for all the interactions that are happening in the material or model. We use the principle of many-body physics and Feynman diagrams to understand and account for all the interactions happening in the material or model.

Once we have a mathematical form of the equation to solve for susceptibility we convert these mathematical equations to a numerical integration code and let the computer do all the calculations for us. Finally, we plot all these results based on what parameters used to compute them. The final results that we obtained are the knight shift or the susceptibility as a function of temperature for different densities of states.

Hence, it illustrates that the new method is working efficiently as expected, and with some further improvement in the setup of the parameters it can make more accurate predictions or results. Once that is accomplished we can use this tool for practical applications to simulate different groups of metallic compounds to study their expected behavior at extreme temperatures.

Bibliography

[1] Xi Chen, JPF LeBlanc, and Emanuel Gull. Simulation of the nmr response in the pseudogap regime of the cuprates. *Nature Communications*, 8(1):14986, 2017.

[2] Elbio Dagotto. Correlated electrons in high-temperature superconductors. *Reviews of Modern Physics*, 66(3):763, 1994.

[3] Giuseppe De Nittis and Max Lein. *Linear response theory: an analytic-algebraic approach*, volume 21. Springer, 2017.

[4] Josef Dick, Frances Y Kuo, and Ian H Sloan. High-dimensional integration: the quasi-monte carlo way. *Acta Numerica*, 22:133–288, 2013.

[5] Marcus Elstner and Gotthard Seifert. Density functional tight binding. *Philosophical Transactions of the Royal Society A: Mathematical, Physical and Engineering Sciences*, 372(2011):20120483, 2014.

[6] W Matthew C Foulkes and Roger Haydock. Tight-binding models and density-functional theory. *Physical review B*, 39(17):12520, 1989.

[7] Jorge E Hirsch. Two-dimensional hubbard model: Numerical simulation study. *Physical Review B*, 31(7):4403, 1985.

[8] K Ishida, H Mukuda, Y Kitaoka, K Asayama, ZQ Mao, Y Mori, and Y Maeno. Spin-triplet superconductivity in sr2ruo4 identified by 17o knight shift. *Nature*, 396(6712):658–660, 1998.

[9] James P.F LeBlanc. libami. `https://github.com/jpfleblanc/libami.git`, 2022.

[10] Gerald D Mahan. *Many-particle physics*. Springer Science & Business Media, 2000.

[11] Richard D Mattuck. *A guide to Feynman diagrams in the many-body problem*. Courier Corporation, 1992.

[12] BDE McNiven, Hanna Terletska, GT Andrews, and JPF LeBlanc. One-and two-particle properties of the weakly interacting two-dimensional hubbard model in proximity to the van hove singularity. *Physical Review B*, 106(3):035145, 2022.

[13] DM Nisson and NJ Curro. Nuclear magnetic resonance knight shifts in the presence of strong spin–orbit and crystal-field potentials. *New Journal of Physics*, 18(7):073041, 2016.

[14] Stephane Pairault, David Senechal, and A-MS Tremblay. Strong-coupling perturbation theory of the hubbard model. *The European Physical Journal B-Condensed Matter and Complex Systems*, 16:85–105, 2000.

[15] Christian P Robert, George Casella, Christian P Robert, and George Casella. Monte carlo integration. *Monte Carlo statistical methods*, pages 71–138, 1999.

[16] Mercè Roig, Astrid T Rømer, Andreas Kreisel, PJ Hirschfeld, and Brian M Andersen. Superconductivity in multiorbital systems with repulsive interactions: Hund's pairing versus spin-fluctuation pairing. *Physical Review B*, 106(10):L100501, 2022.

[17] Otto F Sankey and David J Niklewski. Ab initio multicenter tight-binding model for molecular-dynamics simulations and other applications in covalent systems. *Physical Review B*, 40(6):3979, 1989.

[18] Thomas Schäfer, Nils Wentzell, Fedor Šimkovic IV, Yuan-Yao He, Cornelia Hille, Marcel Klett, Christian J Eckhardt, Behnam Arzhang, Viktor Harkov, François-Marie Le Régent, et al. Tracking the footprints of spin fluctuations: A multi-method, multimessenger study of the two-dimensional hubbard model. *Physical Review X*, 11(1):011058, 2021.

[19] Ramamurti Shankar. *Quantum field theory and condensed matter: An introduction*. Cambridge University Press, 2017.

[20] Amir Taheridehkordi, SH Curnoe, and JPF LeBlanc. Algorithmic matsubara integration for hubbard-like models. *Physical Review B*, 99(3):035120, 2019.